Eur. J. Mineral., 36, 153–164, 2024
https://doi.org/10.5194/ejm-36-153-2024
© Author(s) 2024. This work is distributed under
the Creative Commons Attribution 4.0 License.

European Journal of Mineralogy
Open Access

Heimite, $PbCu_2(AsO_4)(OH)_3 \cdot 2H_2O$, a new mineral from the Grosses Chalttal deposit, Switzerland

Thomas Malcherek[1], **Boriana Mihailova**[1], **Jochen Schlüter**[1], **Philippe Roth**[2], **and Nicolas Meisser**[3]

[1]Mineralogisch-Petrographisches Institut, FB Erdsystemwissenschaften, Universität Hamburg, Grindelallee 48, 20146 Hamburg, Germany
[2]Swiss Seismological Service, ETH Zürich, Sonneggstr. 5, 8092 Zurich, Switzerland
[3]Muséum cantonal des sciences naturelles (Naturéum), Département de géologie, Université de Lausanne, Anthropole, Dorigny, 1015 Lausanne, Switzerland

Correspondence: Thomas Malcherek (thomas.malcherek@uni-hamburg.de)

Received: 21 September 2023 – Revised: 27 November 2023 – Accepted: 2 December 2023 – Published: 30 January 2024

Abstract. The new mineral heimite (IMA2022-019), $PbCu_2(AsO_4)(OH)_3 \cdot 2H_2O$, was found at the Grosses Chalttal deposit, Mürtschenalp district, Glarus, Switzerland, where it occurs as a secondary mineral associated mainly with bayldonite and chrysocolla. Heimite forms lath-like, prismatic transparent crystals of green or pale-blue colour. It has a pale-green streak and a vitreous-to-silky lustre. The calculated density is $4.708\,g\,cm^{-3}$. The empirical formula based on nine O atoms per formula unit is $Pb_{1.04}Ca_{0.03}Cu_{2.10}As_{1.10}H_{6.14}O_9$. Heimite is pseudo-orthorhombic, with monoclinic symmetry; space group $P2_1/n$; and unit cell parameters $a = 5.9132(5)$, $b = 7.8478(6)$ and $c = 16.8158(15)$ Å and $\beta = 90.007(6)°$, $V = 780.33(8)$ Å^3 and $Z = 4$. The five strongest lines in the calculated powder diffraction pattern are (d in Å(I)hkl) as follows: 8.425(100)002, 3.713(60)014, 3.276(54)120, 3.221(42)023 and 2.645(61)016. The crystal structure, refined to $R_1 = 2.75\,\%$ for 1869 reflections with $I > 3\sigma(I)$, is based on chains of edge-sharing, Jahn–Teller-distorted CuO_6 octahedra, laterally connected by AsO_4 tetrahedra and sixfold coordinated Pb atoms. The resulting layers are stacked along [001]. Interlayer hydrogen bonding is mediated by hydrogen atoms that belong to OH groups and to H_2O, mutually participating in the Cu coordination. The crystal structure of heimite is related to that of duftite, and both minerals are found epitactically intergrown at the type locality.

1 Introduction

Among the secondary Cu minerals, several hydrous or basic lead copper arsenates are known, such as duftite, $PbCu(AsO_4)(OH)$; bayldonite, $Cu_3Pb(AsO_4)_2(OH)_2$; plumboagardite, $(Pb,REE,Ca)Cu_6(AsO_4)_3(OH)_6 \cdot 3H_2O$; or thometzekite, $PbCu_2(AsO_4)_2 \cdot 2H_2O$. Common to the crystal structures of these minerals is the presence of edge-sharing, Jahn–Teller-distorted CuO_6 octahedra. The new mineral heimite represents a different structure type with respect to these known compounds, while containing similar Cu coordination as well as stereochemically active Pb^{2+} cations.

The name heimite honours Albert Heim (1849–1937), a Swiss geologist, professor at the ETH Zurich and author of the acclaimed *Geologie der Schweiz* (1919–1922). To explain the anomaly of the stratigraphic column in the Glarus Alps, Heim first advocated the double-fold model (Letsch, 2014). He later (1902) acknowledged his misinterpretation, which, owing to his fame, closed a long, controversial debate and definitely established the Glarus overthrust model, which is central in the history of orogenesis in general and of Alpine geology in particular. The region of the Glarus thrust fault, to which the Grosses Chalttal deposit belongs, was chosen as a UNESCO World Heritage Site in 2008.

The new mineral and its name have been approved by the International Mineralogical Association (IMA2022-019). The holotype (collected by Philippe Roth) is deposited at the Museum der Natur Hamburg – Mineralogie, Leibniz-Institut zur Analyse des Biodiversitätswandels (LIB), Grindelallee 48, 20146 Hamburg, Germany, cata-

Figure 1. Sprays of heimite crystals radially grown on spherical bayldonite aggregates and a chrysocolla crust (photo: Remo Zanelli).

logue number Ro3701. Other heimite-bearing samples, studied for paragenetic association, are conserved at the Département de géologie of the Muséum cantonal des sciences naturelles (Naturéum), UNIL, 1015-Lausanne, Switzerland, catalogue numbers MGL 094490 (cotype) and MGL 087051 to 087070.

2 Occurrence

Heimite was found during the systematic energy-dispersive X-ray spectroscopy (EDXS) screening of material collected on the dump of the Grosses Chalttal deposit, Mürtschenalp district, Glarus, Switzerland (47°04′09.9″ N, 9°11′26.5″ E), in 2003 (Roth, 2022). The analyses showed the presence of Cu, Pb, As and O in element ratios close to those of bayldonite. Since the crystal morphology is however different, a powder X-ray diffraction analysis was performed that showed that the mineral was neither bayldonite nor, probably, an existing species.

The Grosses Chalttal deposit, like all the mines and small deposits that make up the Mürtschenalp district (Bächtiger, 1963), is located in the Helvetic nappes of eastern Switzerland, within the Permian Verrucano formation, which is up to 1000 m thick and consists of layered volcanic rocks, sandstones and conglomerates. During Oligocene–Miocene times, the Verrucano was pushed northwards at least 40 km along the famous Glarus thrust above younger Cretaceous carbonates and Tertiary flysch sediments (Badertscher et al., 2001; Pfiffner, 2014). At Grosses Chalttal, the rock appears in its coarse fanglomeratic sernifite facies (Letsch, 2014), as a pale-grey to greenish breccia.

The Grosses Chalttal Cu and partly U mineralization has a sedimentary origin with at least two phases of later remobilization (Bächtiger, 1963). The primary ore consists mainly, in order of abundance, of tennantite-(Cu), pyrite, bornite, chalcopyrite, galena, uraninite, and brannerite in a quartz and minor baryte matrix. As could be shown by electron microprobe and powder diffraction analysis in the context of this study, primary tennantite-(Cu) is consistently associated with a fine-grained admixture of spionkopite and yarrowite with $(Cu + Ag + Hg)/S = 1.12$ to 1.40 ($Ag \sim 1.0$ at. %; $Hg \sim 0.3$ at. %), which is of secondary (cementation) origin. Molybdenite, stromeyerite and wittichenite are also mentioned as very minor constituents of the primary ore (Bächtiger, 1963). A broad suite of secondary minerals, primarily arsenates and sulfates with only rare carbonates, has been described (Meisser, 1999). Because of the discovery of the type material in the form of a small sample on the mine dumps, contextualization of the occurrence of the new mineral species in the ore body is not possible. Crystals of the new mineral are closely associated with bayldonite spheres and chrysocolla on the holotype (Fig. 1). Cotype crystals are associated with chrysocolla, malachite, azurite, duftite, mimetite, brochantite, euchroite, bayldonite, cerussite, wulfenite, cyanotrichite, strashimirite and parnauite, in decreasing order of frequency.

Table 1. Chemical data (wt %) for heimite.

Constituent	Mean	Range	SD	Probe standard
CuO	28.64	27.26–30.68	1.05	chalcopyrite
PbO	39.89	38.08–41.75	0.93	galena
CaO	0.25	0.03–0.85	0.26	calcite
As_2O_5	21.73	20.39–23.04	0.72	arsenopyrite
$H_2O_{calc.}$*	9.49			
Total	100.00			

* $H_2O_{calc.}$ for a total of 100 wt %.

In addition to its type locality, the Grosses Chalttal deposit, heimite has since also been reported from four other small Pb–Cu ore deposits, all located in the Swiss Alps (Roth, 2022): Hochmättli, also in the Mürtschenalp district, Glarus; Tieftobel, near Schmitten, Grisons; and Collioux Supérieur and Termino, both near Saint-Luc, in Val d'Anniviers, Valais.

3 Appearance and properties

Heimite occurs as sprays of light-pistachio-green, lath-like, prismatic crystals that reach up to 450 µm in length and 40 µm in width (see Fig. 1).

Some, but not all, crystals turn blue under the electron beam of the SEM (Roth, 2022). On certain specimens, crystals showing both changed and unchanged colours occur closely together. A few specimens were found on the mine dump showing blue-coloured crystals when unearthed. Within the accuracy of the EDXS measurements, they show no deviation in their chemical composition with respect to the composition of the colourless to pale-green crystals. Heimite has a pale-green streak, vitreous-to-silky lustre and no observable fluorescence. It shows perfect cleavage on {001}. The calculated density is 4.708 g cm^{-3} based on the unit cell from single-crystal structure determination and an empirical formula with seven hydrogen atoms. Based on the ideal formula (see below) the density is 4.769 g cm^{-3}. Heimite is optically biaxial with a measured 2 V of 87° and calculated $n_{av} = 1.816$. Heimite shows faint pleochroism from faint green ||[100] to bright green ||[010]. The lath-like crystals are dominated by {001}; extend along [100]; and are delimited by {010}, {110} and {100} forms. Heimite readily dissolves in hydrochloric acid.

4 Chemical composition

Electron microprobe analyses were performed using a Cameca SX100 in wavelength-dispersive mode at the Institut für Endlagerforschung, Technische Universität Clausthal, Germany. The analytical conditions were 15 kV accelerating voltage, 30 nA beam current and 5 µm beam diameter for 11 sample spots. Results are given in Table 1.

The available material was insufficient for the direct determination of H_2O content; hence it is calculated based on the difference to 100 wt %. The empirical formula calculated on the basis of nine anions per formula unit is $Pb_{1.04}Ca_{0.03}Cu_{2.1}As_{1.1}H_{6.14}O_9$. Assuming seven hydrogen atoms in agreement with the structure determination (see below), the calculated H_2O content becomes 11.64 wt % and the total increases to 102.15 wt %, resulting in an empirical formula $Pb_{0.97}Ca_{0.02}Cu_{1.95}As_{1.02}H_7O_9$. The ideal formula is $PbCu_2(AsO_4)(OH)_3 \cdot 2(H_2O)$, which requires CuO 28.40 wt %, PbO 39.84 wt %, As_2O_5 20.51 wt % and H_2O 11.25 wt %, totalling 100 wt %.

5 X-ray diffraction and crystal structure

Single crystals of heimite were studied using a Nonius KappaCCD four-circle diffractometer with graphite-monochromated Mo$K\alpha$ radiation. Pixel integration and data reduction were performed with the Eval15 program suite (Schreurs et al., 2010).

The selected light-blue crystal consists of two domains related by 178° rotation about [001]. Unit cell parameters were determined based on the position of 27 019 observed and non-overlapping reflections, arising from both domains. A numerical absorption correction based on crystal morphology was calculated using SADABS (SADABS-2008/1). Non-overlapping reflections from the larger of the two domains, amounting to 92 % of the crystal volume, were used to solve the crystal structure in the orthorhombic space group *Pnma* (no. 62), using the Superflip program (Palatinus and Chapuis, 2007). The structure was refined in this space group setting using Jana2006 (Petříček et al., 2014) with scattering factors for the neutral elements. CrystalMaker (Palmer, 2015) has been used for all structure drawings. In the orthorhombic structure, Pb, As and five oxygen atoms occupy special positions 4c on mirror planes at $y = 1/4$ and $y = 3/4$, whereas Cu and two further oxygen atoms occupy general positions 8d. The edge-sharing, [4 + 2] Jahn–Teller-distorted CuO_6 octahedra are propagated along [010] by the mirror operation of *Pnma*, forming parallel chains along [010]. Each AsO_4 tetrahedron connects two adjacent CuO_6 units of one chain by shared corner oxygens. A third corner of the AsO_4 tetrahedron is shared with CuO_6 units in a parallel chain. Pb atoms occupy the space between the CuO_6 chains, giving rise to corrugated layers normal to [001].

With a given anion charge of 18 and a total non-hydrogen cation charge of 11, charge balance requires the presence of seven H^+ ions. Low bond valence sums (BVSs) indicate the oxygen anions involved in hydrogen bonding, with the three remaining equatorial oxygen ligands of Cu (those not bonded to As) involved in OH groups. Due to its very small BVS, the remaining axial Cu ligand (O_x) can be attributed to a water molecule. The position of hydrogen atoms is either located in difference Fourier maps or, in the case of the H_2O ligand,

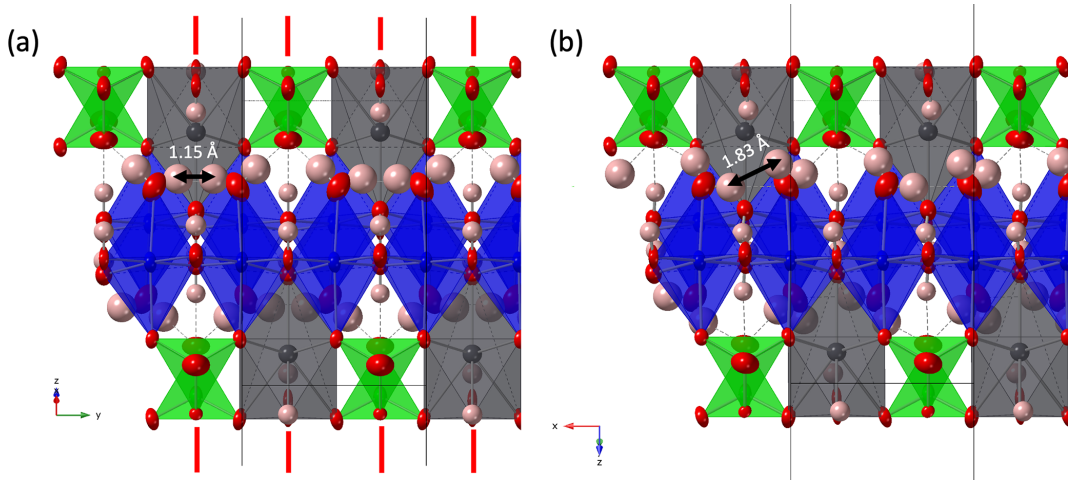

Figure 2. **(a)** Crystal structure of heimite in space group *Pnma* in projection along $[\bar{3}01]$. Displacement ellipsoids are shown at the 90 % probability level. Red lines indicate the position of mirror planes. **(b)** Heimite crystal structure with $P2_1/n$ symmetry projected along $[03\bar{1}]$. As atoms are shown in green, Cu in blue, Pb in grey and O in red colour. Hydrogen atoms are shown as pink spheres.

constructed from triangular coordination of the central O_x atom by Cu and two hydrogen atoms. Isotropic displacement of hydrogen was refined as coupled to the displacement of the oxygen donor atoms, with distance constraints of 1.0 and 0.96 Å for OH^- and H_2O, respectively. The intramolecular angle of H_2O was constrained to 104.5°. In the orthorhombic structure, there would exist only one unique water molecule, with adjacent molecules along the Cu chain related by the mirror operation of *Pnma* (Fig. 2a).

The position of the water molecule is fixed by hydrogen bonding with one of the corner atoms of the AsO_4 tetrahedron. In combination with the mirror operation, this causes the H atoms of neighbouring water molecules to be only 1.15 Å apart. This distance is much shorter than the intramolecular H–H distance, and it can therefore be expected to destabilize such a conformation. That the adjacent water ligands across the mirror plane are attracted to each other by formation of mutual hydrogen bonding, rather than repelled by the close proximity of hydrogen atoms, is indicated by the fact that the corresponding long Cu–O bonds are slightly inclined towards each other (Fig. 2). Because of this, the orthorhombic symmetry is assumed to be broken by the independent orientation of adjacent H_2O ligands and resulting violation of the mirror plane. A suitable subgroup of *Pnma* is $P2_1/n$(no. 14), where ***a*** and ***b*** axes are swapped with respect to the orthorhombic setting. The resulting crystal structure is shown in Fig. 2b. Crystal data and refinement details are summarized in Table 2. The refinement quality of the monoclinic structure is comparable to the orthorhombic setting, with R factors for the orthorhombic structure being even slightly lower. This is due to the X-ray scattering being dominated by lead, with negligible contributions from the symmetry-breaking hydrogen atoms.

Several crystals of light-green colour similar to those shown in Fig. 1 were examined as well. These had a generally smaller size and were of lower quality than the pale-blue crystal described in Table 2, but they rendered very similar results in terms of unit cell size and crystal structure.

In the monoclinic structure, all atoms occupy general Wyckoff positions 4e. Copper is distributed over two different sites Cu1 and Cu2, and the seven oxygen sites of the orthorhombic structure are split into nine sites. Those atoms occupying mirror planes in the orthorhombic structure hardly deviate from these positions, as is shown by the x coordinates of Pb1, As1, O3 to O7 and H4 to H7 being within 2 estimated standard deviations of 1/4 and 3/4 (Table 3).

Most importantly the O_x site of the orthorhombic structure is now split into two sites, O_x1 and O_x2, forming the centres of the two independently oriented water molecules. These are able to form mutual hydrogen bonds, with the short intermolecular H–H distance from the orthorhombic structure increased to 1.83 Å (Fig. 2b). The potential hydrogen bonds and the resulting OH stretching frequencies, calculated using the empirical formula described by Libowitzky (1999), are tabulated in Table 4.

Hydrogen bonds between the water molecules exist between neighbouring molecules along the same chain of Cu atoms (O_x1–O_x2), as well as between molecules belonging to different chains (O_x1–O_x1). Anisotropic displacement factors and selected interatomic distances are shown in Tables 5 and 6, respectively.

Calculated bond valence sums (Table 7) are reasonably close to the formal charges of the ions. One of the corner atoms of the AsO_4 tetrahedron acts as an acceptor anion for several hydrogen bonds (Table 4), thus completing its BVS to 1.85. An overview of the crystal structure in projection along [100], i.e. along the direction of the Cu chains, tantamount to

Table 2. Crystal and structure refinement details.

Diffractometer	Nonius KappaCCD	
Radiation wavelength (Å)	Mo$K\alpha$, $\lambda = 0.7107$	
Structural formula	$PbCu_2(AsO_4)(OH)_3 \cdot 2(H_2O)$	
Crystal system	Monoclinic	Orthorhombic
Space group	$P2_1/n$ (no. 14)	*Pnma* (no. 62)
a (Å)	5.9132(5)	7.8478(6)
b (Å)	7.8478(6)	5.9132(5)
c (Å)	16.8158(15)	16.8158(15)
β (°)	90.007(6)	90
V (Å^3)	780.33(11)	780.33(11)
Z	4	
Density (g cm^{-3})	4.769	
Absorption coefficient (mm^{-1})	31.154	
Crystal size (mm)	$0.27 \times 0.035 \times 0.012$	
T_{min}, T_{max}	0.035, 0.692	
θ_{max} (°)	30	
Obs. criterion	$I > 3\sigma(I)$	
Reflections: total, unique, obs.	26 146, 2269, 1869	25 699, 1237, 1076
R_{int}	0.0566	0.0635
Refinement method	Full matrix least squares on F^2	
R_{obs}, R_{all}	0.0275, 0.0359	0.0248, 0.03
Goodness of fit	1.11	1.12
Parameters, restraints, constraints	140, 9, 7	81, 5, 7
Largest diff. peak/hole (e A^{-3})	2.13/−1.32	2.07/−1.04

Table 3. Atomic positions and equivalent isotropic displacement factors of heimite in SG $P2_1/n$.

Atom	x	y	z	U_{eqv} (Å^2)
Pb1	0.25001(4)	0.83278(3)	0.203979(13)	0.01565(8)
As1	0.74997(8)	0.03728(7)	0.29566(3)	0.00899(14)
Cu1	0.99850(11)	0.69637(9)	0.38968(4)	0.01234(18)
Cu2	0.50146(11)	0.69643(9)	0.38971(4)	0.01218(18)
O1	0.9875(6)	0.0450(5)	0.2394(2)	0.0145(11)
O2	0.5139(6)	0.0455(5)	0.2394(2)	0.0141(11)
O3	0.7504(6)	0.8568(5)	0.3517(3)	0.0134(10)
O4	0.7491(7)	0.5581(5)	0.4277(2)	0.0127(10)
O5	0.7502(8)	0.2091(5)	0.3553(3)	0.0222(12)
O6	0.2496(6)	0.0389(5)	0.0873(2)	0.0144(11)
O7	0.2502(7)	0.8364(5)	0.3522(3)	0.0142(11)
O_x1	0.9750 (9)	0.8358(7)	0.5195(3)	0.0310(17)
O_x2	0.5232(9)	0.8361(7)	0.5190(3)	0.0298(16)
H4	0.740(12)	0.459(7)	0.397(4)	0.0152
H6	0.236(13)	0.044(9)	0.035(3)	0.0173
H7	0.231(12)	0.936(7)	0.378(4)	0.0171
H1O_x1	0.067(14)	0.797(9)	0.561(4)	0.0372
H2O_x1	0.931(14)	0.944(7)	0.535(4)	0.0372
H1O_x2	0.478(11)	0.852(11)	0.571(3)	0.0358
H2O_x2	0.672(9)	0.819(10)	0.522(4)	0.0358

Table 4. Hydrogen bonding of heimite based on the structure model. Calculated OH stretching frequencies (Libowitzky, 1999) are given in the final column.

Donor	Hydrogen	Acceptor	D–H distance (Å)	H···A distance (Å)	D–A distance (Å)	A–H···D angle (°)	Frequency (cm^{-1})
O7	H7	O_x1	0.90(6)	2.77(6)	3.612(7)	156(6)	3592
O4	H4	O5	0.94(6)	2.08(5)	2.998(6)	165(5)	3550
O6	H6	O4	0.89(5)	1.97(5)	2.789(6)	153(6)	3386
O_x1	$H1O_x1$	O5	0.94(7)	1.77(7)	2.683(7)	163(6)	3133
O_x1	$H2O_x1$	O7	0.93(6)	2.78(7)	3.612(7)	150(5)	3592
O_x1	$H2O_x1$	O_x1	0.93(6)	2.03(6)	2.675(7)	125(6)	3104
O_x2	$H1O_x2$	O5	0.92(5)	1.89(6)	2.685(7)	143(6)	3140
O_x2	$H2O_x2$	O_x1	0.89(5)	1.80(5)	2.672(8)	166(8)	3093

Table 5. Anisotropic displacement factors of heimite in square ångströms ($Å^2$).

Atom	U^{11}	U^{22}	U^{33}	U^{12}	U^{13}	U^{23}
Pb1	0.01590(13)	0.01546(13)	0.01560(13)	−0.00008(7)	−0.00054(8)	0.00056(7)
As1	0.0065(2)	0.0101(3)	0.0104(2)	−0.00009(17)	−0.00038(19)	0.00095(18)
Cu1	0.0066(3)	0.0142(3)	0.0163(3)	0.0001(2)	0.0007(2)	0.0038(2)
Cu2	0.0069(3)	0.0137(3)	0.0159(3)	−0.0004(2)	−0.0014(2)	0.0037(2)
O1	0.0084(18)	0.019(2)	0.0160(19)	0.0016(14)	0.0012(15)	0.0048(15)
O2	0.0077(17)	0.0167(19)	0.0180(19)	−0.0017(14)	−0.0043(15)	0.0016(15)
O3	0.0074(17)	0.0150(17)	0.018(2)	−0.0004(14)	0.0008(15)	0.0106(15)
O4	0.0105(17)	0.0132(17)	0.0143(19)	−0.0005(14)	−0.0017(14)	0.0018(15)
O5	0.034(2)	0.0136(19)	0.019(2)	0.0004(18)	−0.0035(18)	−0.0027(17)
O6	0.0115(18)	0.019(2)	0.0126(18)	−0.0001(15)	−0.0018(15)	−0.0039(15)
O7	0.0041(16)	0.0125(18)	0.026(2)	0.0014(13)	−0.0015(16)	0.0035(15)
O_x1	0.027(3)	0.035(3)	0.031(3)	−0.005(2)	−0.012(2)	0.006(2)
O_x2	0.024(3)	0.035(3)	0.031(3)	0.003(2)	0.008(2)	0.003(2)

Table 6. Selected bond distances in ångströms (Å).

Pb1–O1	2.353(4)	Cu1–O3	2.036(4)
Pb1–O1	2.901(4)	Cu1–O4	1.940(4)
Pb1–O2	2.362(4)	Cu1–O6	1.973(4)
Pb1–O2	2.903(4)	Cu1–O7	1.955(4)
Pb1–O6	2.543(4)	Cu1–O2	2.473(4)
Pb1–O7	2.492(5)	Cu1–O_x1	2.446(5)
⟨Pb–O⟩	2.5920	⟨Cu1–O⟩	2.1372
As1–O1	1.694(4)	Cu2–O3	2.040(4)
As1–O2	1.687(4)	Cu2–O4	1.932(4)
As1–O3	1.701(4)	Cu2–O6	1.970(4)
As1–O5	1.680(4)	Cu2–O7	1.952(4)
⟨As–O⟩	1.6905	Cu2–O1	2.476(4)
		Cu2–O_x2	2.439(5)
		⟨Cu2–O⟩	2.1348

the extension direction of the prismatic crystals, is shown in Fig. 3. The weakly bonded layers are stacked along [001], in agreement with the orientation of the cleavage planes.

Pb is coordinated by six oxygen atoms in a strongly distorted, trigonal antiprismatic coordination environment (Fig. 4). The asymmetric nature of the coordination, with Pb significantly displaced from its centre, indicates stereochemical activity of the Pb^{2+} lone-pair electrons in heimite. Each of the bond valences with two further oxygen atoms at the corners of two adjacent AsO_4 tetrahedra (O5, Fig. 4) at a distance of approximately 3.27 Å contributes less than 4 % to the formal charge of Pb^{2+} (Table 7).

Following the definition given by Wildner et al. (2014), the tetragonality factor, $T = \langle Cu–O\rangle_{eq}/\langle Cu–O\rangle_{ax}$, of the two CuO_6-coordination polyhedra is nearly identical and amounts to 0.8. Due to the aforementioned tilting of the Cu–O_xH_2 bonds, the angle between the two axial ligands of the Cu atom is not 180° but 174.67(15)° for Cu1 and 175.05(15)° for Cu2, respectively.

Powder diffraction

Due to the scarcity of available sample material, powder diffraction measurements of heimite were performed using an aggregate of randomly oriented heimite crystals glued to the tip of a glass fibre and rotated by Gandolfi-type motion on the single-crystal diffractometer described above. Several background-subtracted scans were added to obtain the

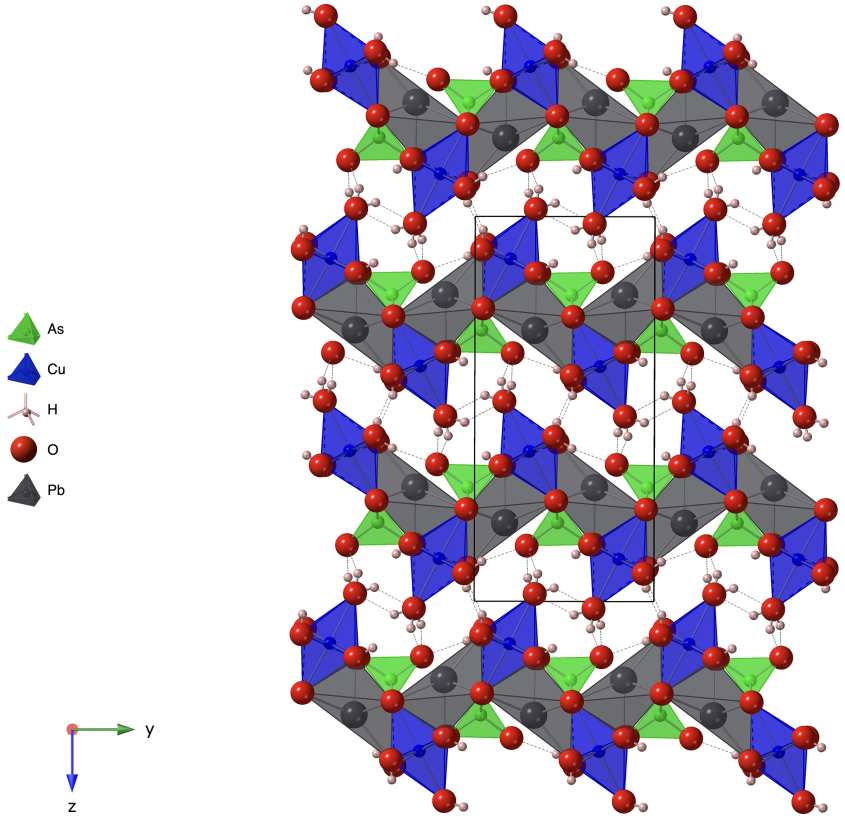

Figure 3. Crystal structure of heimite in projection along [100].

Table 7. Bond valences of heimite. Bond valence parameters are taken from Gagné and Hawthorne (2015) for Pb–O, As–O and Cu–O and from Malcherek and Schlüter (2007) for H–O.

	Cu1	Cu2	As1	Pb1	H4	H6	H7	H1O$_x$1	H2O$_x$1	H1O$_x$2	H2O$_x$2	$\sum$
O1	0.11		1.22	0.48 0.14	0.03		0.02					2.00
O2		0.11	1.25	0.47 0.14	0.03		0.02					2.02
O3	0.37	0.37	1.20							0.02	0.02	1.98
O4	0.49	0.50			0.75	0.14					0.04	1.92
O5			1.27	0.06 0.06	0.10			0.17	0.02	0.14	0.02	1.85
O6	0.45	0.45		0.32	0.02	0.82						2.06
O7	0.47	0.47		0.35			0.81		0.03			2.13
O$_x$1	0.12						0.05	0.75	0.77 0.11		0.16	1.96
O$_x$2		0.12				0.02	0.04	0.03	0.04	0.78 0.02	0.82	1.87
$\sum$	2.01	2.03	4.94	2.03	0.93	0.98	0.94	0.95	0.97	0.96	1.04	

Table 8. X-ray powder diffraction data (d in Å) for heimite. The five strongest lines are shown in bold typeface.

I_{meas}	I_{calc}	d_{meas}	d_{calc}	hkl
27	**100**	**8.419**	**8.425**	**002**
22	24	7.323	7.126	011
11	21	5.608	5.749	012
	32		5.590	101
	14		4.570	013
	14		4.556	111
7	34	4.143	4.126	112
8	18	3.942	4.076	103
	27		3.932	020
	18		3.829	021
30	**60**	**3.729**	**3.713**	**014**
	27		3.619	113
100	**54**	**3.185**	**3.276**	**120**
	42		**3.221**	**023**
	38		3.216	121
	40		3.146	114
45	41	2.925	3.053	122
	24		2.963	200
	25		2.874	024
	25		2.830	123
45	36	2.765	2.795	202
	32		2.745	115
53	**61**	**2.642**	**2.645**	**016**
	40		2.633	212
31	16	2.550	2.590	031
	14		2.586	124
	10		2.486	213
10	16	2.428	2.423	204
	27		2.415	116
	40		2.375	033
37	35	2.345	2.343	221
	23		2.316	214
	13		2.306	132
13	16	2.258	2.278	222
12	22	2.161	2.145	117
19	18	2.080	2.083	134
	18		2.069	035
	16		2.063	224
	20		2.053	027
	12		2.038	206
21	10	1.946	1.962	301
	22		1.953	041
	10		1.940	127
	16		1.924	118
	10		1.912	232
26	12	1.855	1.868	312
	32		1.856	043
	16		1.855	141
	10		1.853	233
	15		1.823	136
	11		1.822	142
	12		1.813	313
54	10	1.751	1.779	234
	26		1.773	037
	15		1.772	128
	10		1.771	143
	23		1.765	320
	16		1.755	321
2	17	1.737	1.744	314
	16		1.727	322
	23		1.717	208
16	40	1.692	1.696	235
	23		1.685	0.0.10
	11		1.684	323
	25		1.677	218
33	14	1.629	1.665	315
	29		1.630	241
	14		1.625	129
	11		1.609	236
9	15	1.573	1.582	316
2	20	1.550	1.523	039
	16		1.523	047
13	22	1.518	1.521	237
	13		1.499	317
	15		1.498	1.2.10
16	30	1.475	1.481	400
	10		1.477	334
	15		1.467	153
	11		1.459	402
18	10	1.385	1.417	318
	12		1.388	1.2.11
	17		1.386	155

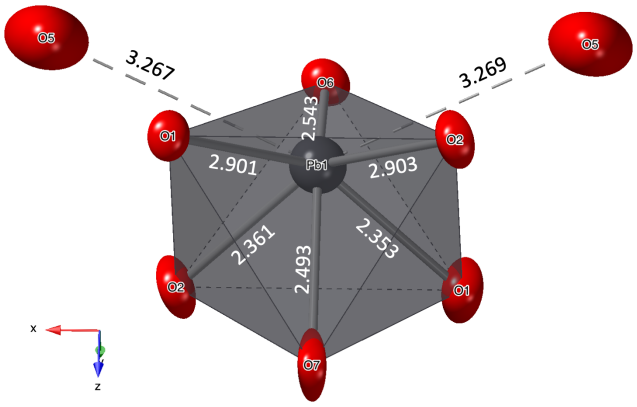

Figure 4. Coordination of the Pb atom. Displacement ellipsoids are shown at the 90 % probability level. Distances are given in ångströms (Å).

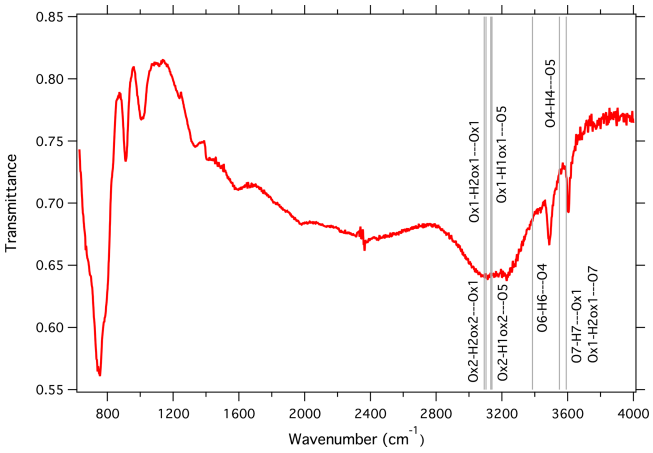

Figure 5. Infrared absorption spectrum of heimite. Vertical lines indicate the calculated positions of OH stretching bands from hydrogen bonding as given in Table 4.

final diffraction image. Diffraction data were integrated using the Nonius Powderize software (Hooft, 2000). The resulting diffractogram was peak-fitted using 27 Gaussian peak shapes up to $2\theta = 32°$ in Igor Pro 9.02. Relative peak intensities and positions are compared in Table 8 with those calculated using Jana2006 from the crystal structure data. Only lines with calculated intensities exceeding 10 % are shown, and split reflections nominally arising from the monoclinic symmetry have been merged. Le Bail refinement (Le Bail, 2005) of the measured powder diffractogram in SG $P2_1/n$ with $\beta = 90°$ and Gaussian peak profiles results in unit cell parameters of $a = 5.967(5)$, $b = 7.896(6)$ and $c = 16.779(16)$ Å and $V = 790.5(9)$ Å^3.

6 Infrared spectroscopy

An infrared transmission spectrum of a single crystal of heimite (Fig. 5) has been collected in the range 630–7000 cm^{-1} using a Bruker VERTEX 70 FTIR spectrometer with a HYPERION 2000 IR microscope and a liquid-nitrogen-cooled mercury cadmium telluride detector. The crystal, approximately 0.01 mm in thickness, was oriented with (001) facing towards the IR beam.

Sharp absorption signals occur at 750, 912, 1010, 3489 and 3606 cm^{-1}. A broad signal appears between 2800 and 3400 cm^{-1}. Comparison with the empirically calculated frequencies given in Table 4 indicates that the highest-frequency fundamental absorption peak at 3606 cm^{-1} would be compatible with OH stretching involved in the longest hydrogen bonding between Ox1 and O7 (3592 cm^{-1}) as well as that between O4 and O5 (3550 cm^{-1}). The other sharp signal at 3489 cm^{-1} might be attributable to hydrogen bonding O6-H6···O4 (3386 cm^{-1}). Several other hydrogen bonds would give rise to OH stretching signals around 3100 cm^{-1}. These all involve the water molecules centred at O_x1 and O_x2 and would fall into the frequency range of the observed broad absorption signal between 2800 and 3400 cm^{-1}. Broadening of this absorption signal may be attributed to displacement or disorder of the water molecules, as is indicated by the displacement ellipsoids of O_x1 and O_x2, which are significantly larger than the corresponding ellipsoids of O1 and O2, i.e. the anions at the opposite side of the CuO_6 coordination, which are stabilized by additional bonding to the As atom. The intense absorption signal at 750 cm^{-1} is similarly observed in other arsenate minerals such as bayldonite, duftite or mimetite, as documented in reference spectra of the RRUFF project (Lafuente et al., 2015).

7 Discussion

7.1 Origin and formation of heimite

It is worth noting that euchroite, a particularly rare copper arsenate, is present at Grosses Chalttal, the type locality of heimite. Euchroite is a metastable mineral of recent formation (Magalhães et al., 1988; Majzlan et al., 2017), and hence, heimite might also be a metastable, geologically young mineral. This could explain its rarity and its late discovery, in spite of its simple chemical composition.

Deep oxidation zones, rich in large and well-crystallized supergene minerals, did not form in the central Alps. This fact is probably related to the powerful glacial erosion of these parts of the Alps during the last 400 000 years, which precludes the formation and preservation of large gossans and the crystallization of supergene mineral species in large crystals.

The supergene mineral association of the second discovery site of heimite, at Hochmättli, located only 2.1 km southwest of the type locality of Grosses Chalttal, has undergone radiometric dating. Two age determinations of the supergene Cu–U–arsenate metazeunerite from Hochmättli us-

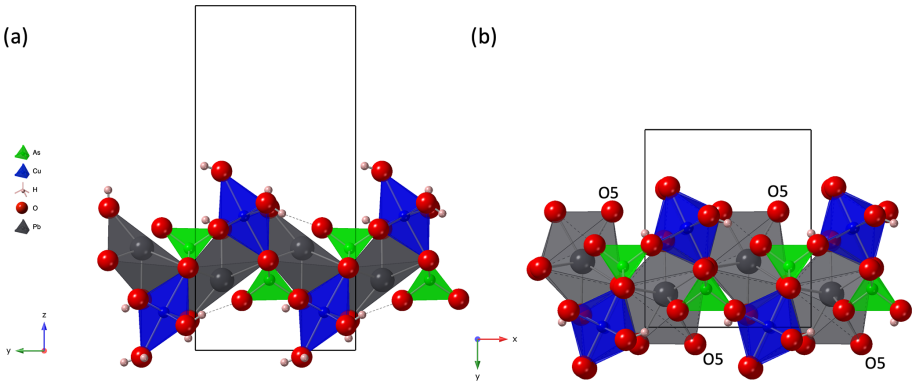

Figure 6. (a) A single layer of the crystal structure of heimite, in projection along [100], compared to **(b)** a corresponding fragment of the duftite crystal structure (Callegari et al., 2017; ICSD no. 25456) in projection along [001]. Black lines show outlines of the respective unit cells.

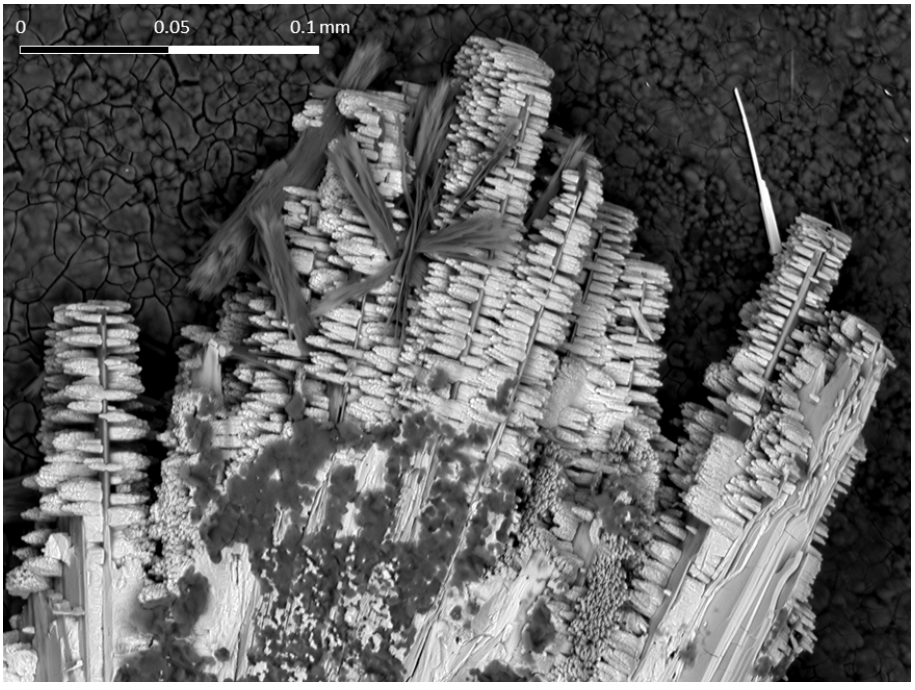

Figure 7. SEM photograph of prismatic duftite crystals grown on tabular heimite. Sample from Grosses Chalttal deposit. The dark-grey, lath-like crystals are malachite, the bright needle towards the top right is mimetite.

ing the ^{238}U–^{234}U–^{230}Th disequilibrium method (with the UV-LA-MC-ICP-MS technique) indicate ages of the Middle Pleistocene of 209.09 (3.93) and 210.06 (2.97) Ka (Meisser, 2012). These ages correspond to the Mindel–Riss interglacial period, which locally represents the interglacials of the Meikirch complex (Preusser et al., 2005, 2011). The formation of these supergene minerals would have resulted from combined physical and chemical phenomena that affected the hypogene mineralizations, namely strong fracturing of the rock substrate due to decompression, following partial melting of the glacial ice cap and the circulation of oxidizing meteoric water, responsible for the formation of supergene minerals. This genetic process is particularly well documented in the uranium mineral deposits of the central Alps (Meisser, 2012). In central Europe, outside the Alpine arc and the related intense Quaternary glacial phenomena, the few available age determinations of secondary minerals show older ages, ranging from 0.5 to 4 million years (Dill et al., 2010).

7.2 Crystal structure of heimite

To our knowledge heimite represents a unique structure type for basic lead copper arsenates. The crystal structure is composed of layers connected by hydrogen bonding. Part of the

bonding is mediated by water molecules, stored between the layers. In the absence of some of the water molecules forming the sixths ligand of the Cu-coordination environment of heimite, there would be no need for the crystal structure to distort to monoclinic symmetry. The monoclinic distortion is therefore expected to be stronger in particularly well ordered samples and to increase with falling temperature. As the removal of water molecules is charge neutral, it is possible that some O_x sites become partially unoccupied, leaving Cu locally in a five-coordinated, square pyramidal coordination environment. The observed colour changes from green to blue colour, especially under electron irradiation in the SEM but also in some of the as-found crystals, could be related to the partial dehydration of heimite samples. Numerous secondary Cu minerals are known to support square pyramidal, $[4+1]$ Cu coordination. Among these are many deep-blue minerals like clinoclase, $Cu_3(AsO_4)(OH)_3$ (see also Eby and Hawthorne, 1990, for other examples of this coordination), or azurite, $Cu_3(CO_3)_2(OH)_2$ (Gattow and Zemann, 1958), where one of the two Cu-coordination environments is a square pyramid of oxygen atoms.

The unique crystal structure of heimite is related to the structure of duftite, $PbCu(AsO_4)(OH)$. The thickness of a single heimite layer is about 9.3 Å, which approximately matches the dimension of the *b* unit cell parameter of duftite (Callegari et al., 2017). Moreover, its *a* and *c* parameters are similar to the *b* and *a* unit cell parameters of heimite, respectively. In fact, the crystal structure of duftite can be obtained from that of heimite by removing one $Cu(OH)_2 \cdot 2H_2O$ per formula unit and stacking the mutually shifted, altered heimite layers (see Fig. 6). Note that the equivalent atoms of O5 in duftite (Fig. 6b) would belong to layers of the heimite structure adjacent to the one shown in Fig. 6a (cf. Fig. 3), where they constitute the "free" corner atoms of the AsO_4 tetrahedra. Thus, the coordination number of Pb in duftite is higher and Pb coordination is more regular than in heimite. Moreover, the tetragonal elongation of the CuO_6 octahedra is at 45° angles to the Cu chains in duftite, whereas it is normal to them in heimite (Fig. 6).

Figure 7 shows an SEM image of a cotype specimen with prismatic duftite crystals that grow on tabular heimite crystals. With [001] as the likely elongation direction of the duftite crystals, parallel to the chains of edge-sharing CuO_6 octahedra, it follows that $(001)_{Him}||(001)_{Dft}$. Thus the Cu-chain directions of the two minerals should be normal to each other. The observation of duftite growing on heimite crystals again might hint at the metastability of heimite, possibly preceding the formation of the more common duftite.

8 Conclusions

Heimite is a hydrous, basic copper–lead–arsenate that is structurally related to duftite and the adelite–descloizite group of minerals. Cu coordination in partially dehydrated heimite may locally vary between sixfold, $[4+2]$ distorted and fivefold, square pyramidal. The mineral has so far been found at various locations in the Swiss Alps, but it is expected to occur as a supergene mineral in Cu deposits in other locations too.

Data availability. Crystallographic data for heimite are available in the Supplement.

Supplement. The supplement related to this article is available online at: https://doi.org/10.5194/ejm-36-153-2024-supplement.

Author contributions. PR, NM and JS initiated the project, with PR and NM providing samples and preliminary analysis. TM, BM and PR performed experiments. The manuscript was written by TM with contributions by all co-authors.

Competing interests. The contact author has declared that none of the authors has any competing interests.

Disclaimer. Publisher's note: Copernicus Publications remains neutral with regard to jurisdictional claims made in the text, published maps, institutional affiliations, or any other geographical representation in this paper. While Copernicus Publications makes every effort to include appropriate place names, the final responsibility lies with the authors.

Special issue statement. This article is part of the special issue "New minerals: EJM support". It is not associated with a conference.

Acknowledgements. Microprobe analysis of the holotype was kindly carried out by Dietlind Nordhausen at TU Clausthal, Germany. Some of the studied samples were collected in 1984 by Thomas Mumenthaler and Walter Cabalzar (deceased). Comments by Alan Pring and the anonymous reviewer helped to improve the manuscript.

Financial support. The characterization and preservation of the mineral paragenesis of heimite have benefited from funding by the Swiss Academy of Sciences (SCNAT) through SwissCollNet project no. SCN201-VD to Nicolas Meisser.

Review statement. This paper was edited by Cristiano Ferraris and reviewed by Alan Pring and one anonymous referee.

References

Bächtiger, K.: Die Kupfer- und Uranmineralisationen der Mürtschenalp (Kt. Glarus, Schweiz), Beiträge zur Geologie der Schweiz, Geotechnische Serie, Lieferung 38, 113 pp., https://doi.org/10.3929/ethz-a-000088857, 1963.

Badertscher, N. P., Beaudoin, G., Therrien, R., and Burkhard, M.: Glarus overthrust: A major pathway for the escape of fluids out of the Alpine orogen, Geology, 30, 875–878, 2001.

Callegari, A. M., Boiocchi, M., Zema, M., and Tarantino, S. C.: Crystal structure refinement of duftite, $PbCu(AsO_4)(OH)$, from Grube Clara, Oberwolfach, Schwarzwald, Germany, Neues Jb. Miner. Abh., 194, 157–164, 2017.

Dill, H. G, Gerdes, A., and Weber, B.: Age and mineralogy of supergene uranium minerals – tools to unravel geomorphological and palaeohydrological processes in granitic terrains (Bohemian Massif, SE Germany), Geomorphology, 117, 44–65, 2010.

Eby, R. K. and Hawthorne, F. C.: Clinoclase and the Geometry of [5]-Coordinate Cu^{2+} in Minerals, Acta Crystallogr. C, 46, 2291–2294, 1990.

Gagné, O. C. and Hawthorne, F. C.: Comprehensive derivation of bond-valence parameters for ion pairs involving oxygen, Acta Crystallogr. B, 71, 562–578, 2015.

Gattow, G. and Zemann, J.: Neubestimmung der Kristallstruktur von Azurit, $Cu_3(OH)_2(CO_3)_2$, Acta Crystallogr., 11, 866–872, 1958.

Hooft, R. W. W.: Powderize, Bruker AXS BV, 2000.

Lafuente, B., Downs, R. T., Yang, H., and Stone, N.: The power of databases: the RRUFF project, in: Highlights in Mineralogical Crystallography, edited by: Armbruster, T. and Danisi, R. M., W. De Gruyter, Berlin, Germany, 1–30, https://doi.org/10.1515/9783110417104, 2015.

Le Bail, A.: Whole powder pattern decomposition methods and applications: A retrospection, Powder Diffr., 20, 316–326, 2005.

Letsch, D.: The Glarus Double Fold: a serious scientific advance in mid nineteenth century Alpine Geology, Swiss J. Geosci., 107, 65–80, 2014.

Libowitzky, E.: Correlation of O-H Stretching Frequencies and O-H···O Hydrogen Bond Lengths in Minerals, Monatsh. Chem., 130, 1047–1059, 1999.

Magalhães, M. C. F., De Jesus, J. D. P., and Williams, P. A.: The chemistry of formation of some secondary arsenate minerals of Cu(II), Zn(II) and Pb(II), Miner. Mag., 52, 679–690, 1988.

Majzlan, J., Števko, M., Dachs, E., Benisek, A., Plášil, J., and Sejkora, J.: Thermodynamics, stability, crystal structure, and phase relations among euchroite, $Cu_2(AsO_4)(OH) \cdot 3H_2O$, and related minerals, Eur. J. Mineral., 29, 5–16, https://doi.org/10.1127/ejm/2017/0029-2584, 2017.

Malcherek, T. and Schlüter, J.: $Cu_3MgCl_2(OH)_6$ and the bond-valence parameters of the OH–Cl bond, Acta Crystallogr. B, 63, 157–160, 2007.

Meisser, N.: Les minéraux d'altération des indices de cuivre et uranium de la Mürtschenalp (SG/GL), Le Cristallier Suisse, 11, 489–503, 1999 (in French and German).

Meisser, N.: La minéralogie de l'uranium dans le massif des Aiguilles Rouges, Matér. Géol. Suisse, Sér. géotech., 96, 1–183, 2012.

Palatinus, L. and Chapuis, G.: Superflip – a computer program for the solution of crystal structures by charge flipping in arbitrary dimensions, J. Appl. Crystallogr., 40, 786–790, 2007.

Palmer, D.: Visualization and analysis of crystal structures using CrystalMaker software, Z. Kristallogr., 230, 559–572, 2015.

Petříček, V., Dušek, M., and Palatinus, L.: Crystallographic Computing System JANA2006: General features, Z. Kristallogr., 229, 345–352, 2014.

Pfiffner, A. O.: Geology of the Alps, Wiley-Blackwell, Chichester, 376 pp., 2014.

Preusser, F., Drescher-Schneider, R., Fiebig, M., and Schlüchter, C.: Re-interpretation of the Meikirch pollen record, Swiss Alpine Foreland, and implications for Middle Pleistocene chronostratigraphy, J. Quaternary Sci., 20, 607–620, 2005.

Preusser, F., Graf, H. R., Keller, O., Krayss, E., and Schlüchter, C.: Quaternary glaciation history of northern Switzerland, E&G Quaternary Sci. J., 60, 21, https://doi.org/10.3285/eg.60.2-3.06, 2011.

Roth, P.: Heimit, ein unerwartetes, weltweit neues Mineral von einer vermeintlich bescheidenen Fundstelle, Schweizer Strahler, 4, 2–9, 2022 (in French and German).

Schreurs, A. M. M., Xian, X., and Kroon-Batenburg, L. M. J.: EVAL15: a diffraction data integration method based on ab initio predicted profiles, J. Appl. Crystallogr., 43, 70–82, 2010.

Wildner, M., Giester, G., Kersten, M., and Langer, K.: Polarized electronic absorption spectra of colourless chalcocyanite, $CuSO_4$, with a survey on crystal fields in Cu^{2+} minerals, Phys. Chem. Minerals, 41, 669–680, 2014.